Final Report

**Establishing Inspection Periods and Preliminary Recommendations for Preventive Measures for Mid-Rise Buildings
Near Coastal and Inland South Florida Environments**

Project Lead: Atorod Azizinamni

Kingsley Lau,
Samanbar Permeh,
Mansoureh Shahabi Ghahfarokhi,
Sepehr Faridmarandi

June 2, 2023

EXECUTIVE SUMMARY

The research sought to provide recommendations for time of inspection of reinforced concrete structural elements susceptible to carbonation-induced concrete and its repair. Recent occurrences of high visibility structural failures have spurred interest to revisit inspection and repair of aging reinforced concrete structures. Corrosion induced by carbonation of the concrete and its pore water can occur in many environments including structures in both wet and dry exposures. This type of corrosion can become increasingly relevant in residential buildings as housing structures age to where sufficient carbonation occurs at reinforcing steel depths. The risk of corrosion for the embedded reinforcing steel in residential buildings can vary depending on several inter-related factors that include the structural design, its materials, and its environmental exposure. The risk of corrosion furthermore can be separated into two phases; 1) corrosion initiation where atmospheric carbon dioxide diffuses into the concrete cover and lowering the beneficial high pore water pH by consuming OH- to allow steel passivation and 2) corrosion propagation where the active corrosion continues at an adequate rate to cause structural damage.

The concrete cast with the different water-to-cement ratio, limestone aggregate size, and conditioned in various moisture environments had different electrical and acoustic characteristics that are inter-related with the concrete microstructure and internal moisture content. These parameters have impact to the extent of concrete carbonation and the extent of corrosion activity. The concrete specimens conditioned in the 95%RH and soak/100%RH conditions maintained in extended accelerated carbonation conditioning for up to 1 month of continuous carbonation of near 100% CO_2 at 20 psi did not yield any significant carbonation penetration due to the slow rate of CO_2 penetration through the pore water. It was evident that additional time was required for concrete carbonation. Concrete carbonation for the concrete specimens maintained in the dry condition fully carbonated within 67 hours in 100% CO_2 environments at 20 psi. Significant concrete carbonation occurred for the concrete specimens maintained at 75%RH. In the dry indoor laboratory conditions, the corrosion rate of steel in the non-carbonated concrete was measured to be on average ~0.01 uA/cm^2. In the carbonated concrete, the corrosion rate ranged from 0.2-0.8 uA/cm^2. From Faradaic conversion, these rates correspond to steel loss of up to 0.001 mm\yr corrosion. In presence of the 42 kip external compressive force, the corrosion rates were similar;

however, the time to corrosion initiation was delayed in time by a factor of 1.6-2. It is evident that both corrosion initiation and propagation should be considered when establishing recommendations for structural health monitoring and inspection.

A test bed for concrete retrofit of carbonated concrete with actively corroding reinforcing steel and instrumentation for corrosion monitoring was developed. Shell repair including the use of UHPC can be implemented for additional study. A novel insitu water pressure drop test has been demonstrated to be sensitive to the internal moisture content of the concrete. Models based on mass and energy conservation have been developed to predict the water pressure drop for concrete with different materials and environmental exposure and ideally can be used to identify concrete characteristics related to permeability and thus susceptibility to carbonation. Insitu non-destructive testing can be employed for concrete inspections for concrete durability. Among those, testing to assess concrete permeability, carbonation, and corrosion rates should be considered.

In summary it should be noted that because of the time limitation of the project, accelerated corrosion tests were conducted. As noted before, ".. The concrete specimens conditioned in the 95%RH and soak/100%RH conditions maintained in extended accelerated carbonation conditioning for up to 1 month of continuous carbonation of near 100% CO_2 at 20 psi did not yield any significant carbonation penetration due to the slow rate of CO_2 penetration through the pore water.". Therefore it could be concluded that under atmospheric conditions, much longer time will be needed to start the carbon induced corrosion. As a result, there is a need to conduct similar tests at atmospheric pressure, which is more representative of the condition, that constructed building are exposed to.

Research team, is also undertaking additional tasks, in the form of wrapping concrete columns constructed using low quality concrete, with advanced cementations materials, namely ultra-High Performance Concrete (UHPC). This report provides details of such tests, which are beyond scope of this project. Nevertheless, this aspect of study will continue using other resources. It is anticipated that in early Fall 2023, the research team will be organizing a workshop to present various methods for proactively protect deficient concrete columns against corrosion and strengthening them where it is needed.

TABLE OF CONTENTS

1. INTRODUCTION

1.1 Background

The research project sought to provide recommendations for time of inspection of reinforced concrete structural elements susceptible to carbonation-induced concrete and its repair with ultra-high performance concrete. Recent occurrences of high visibility structural failures have spurred interest to revisit inspection and repair of aging reinforced concrete structures. Chloride-induced corrosion can cause premature damage of structures in coastal regions. Corrosion induced by carbonation of the concrete and its pore water, on the other hand can occur in many other environments including structures in both wet and dry exposures. This type of corrosion can become increasingly relevant in residential buildings as housing structures age to where sufficient carbonation occurs at reinforcing steel depths. The risk of corrosion for the embedded reinforcing steel in residential buildings can vary depending on several inter-related factors that include the structural design, its materials, and its environmental exposure. The risk of corrosion furthermore can be separated into two phases; 1) corrosion initiation where atmospheric carbon dioxide diffuses into the concrete cover and lowering the beneficial high pore water pH by consuming OH- to allow steel passivation and 2) corrosion propagation where the active corrosion continues at an adequate rate to cause structural damage. It is evident that both corrosion initiation and propagation should be considered when establishing recommendations for structural health monitoring and inspection. Repair of corrosion damaged reinforced concrete structures with UHPC has been suggested due to the growing interest in the material and its beneficial mechanical and material characteristics such as high compressive strengths and low permeability.

1.2 Literature Review

Angst et al., (2018) [1] completed a comprehensive review on the corrosion rate of carbon steel in carbonated concrete, parsing the various published research on varied concrete materials, laboratory test setup and electrochemical corrosion testing. The European standard on concrete EN 206-1 (2000)[2] classifies the risk of carbonation-induced corrosion by the aggressivity of the exposure environment and provides recommendations for water-to-cement ratio (w/c), cement

content, and cover depth. The binder concrete composition and mix design was generally regarded as a major factor to provide adequate structural service life. The main exposure conditions that influence the carbonation-induced corrosion rate include the relative humidity and wet/dry cycling. Due to widely variable exposure conditions, carbonation-induced corrosion rates for steel in concrete ranged from 0.002 $\mu A/cm^2$ to 20 $\mu A/cm^2$. Maximum rates are observed when the concrete is exposed to atmospheres with relative humidity in the range from 55 to 75%. Several authors, relate the corrosion rate primarily to resistive or ohmic control. Concrete porosity, capillary condensation of water vapor, moisture content, and oxygen diffusion also affect the corrosion rate.

1.2.1 Ultra-High Performance Concrete

UHPC has superior compressive and tensile strength, as well as excellent post-cracking and durability characteristics. UHPC obtains high compressive strengths and low permeability due to its low water-to-cement ratio (less than 0.25), use of pozzolanic supplemental cementitious materials, and optimized packing of its granular constituents. The development of these concretes have been facilitated with the advent of high range water reducers and viscosity modifying admixtures. The high quality of the concrete provide excellent bulk characteristics that enhance material durability.

Russel and Graybeal, (2013)[3] reported on the durability of UHPC. Testing by the authors following ASTM C1202[4] resulted in total electrical charge values less than 40 coulombs for steam-cured specimens and 360 coulombs for untreated specimens at 28 days. Others also reported negligible charge values (<100 coulombs) for UHPC. Reported chloride diffusivity values in UHPC were reported to be in the order of 10-13 m2/s.

Shahrokhinasab and Garber, (2021)[5] assessed the durability of non-proprietary UHPC in terms of electrical resistivity, concrete shrinkage, and the effect of fiber clumping. Electrical resistivity testing conformed to ASTM C1760-12[6] to identify resistance to penetration of chloride ions. Testing included both 4-point surface resistivity and 2-point bulk resistivity testing. Shrinkage testing conformed to ASTM C157-17[7] to identify length change of hardened concrete. A vibrating strain gage was used to measure strain due to shrinkage. The non-proprietary UHPC mixes

typically had resolved bulk resistivity exceeding 10 kohm-cm and proprietary UHPC having even better performance. The researchers noted lower resistivity values for mixes with the presence of steel fibers, similar to that noted by Valikhani and Lau, (2021)[8], where fiber content and fiber orientation appeared to affect the resolved electrical resistance. Concrete shrinkage testing provided some indication that higher concentrations of synthetic fibers decreased the total shrinkage strain. Fiber clumping was generally observed more frequently in non-proprietary mixes using synthetic fibers than steel fibers when fibers were rapidly added to the mixer and when long and heavy fibers were used. The fiber clumping typically resulted in lower compressive strength.

Floyd et al., (2020)[9] also reviewed the durability of non-proprietary UHPC. Their review of the literature likewise indicated good durability in terms of chloride penetration and freeze-thaw resistance. A study by Chunping and al., (2016)[10], although indicating good performance of UHPC, did show that heat curing can introduce microcracks that can allow preferential chloride ion penetration and regions for spalling in freeze-thaw testing. Looney et al., (2022)[11] evaluated the corrosion and freeze-thaw durability of concrete repairs with UHPC including small scale test specimens conforming to ASTM C1202 [4] and ASTM C666 [12] and large scale anodic galvanostatic accelerated corrosion testing using extracted reinforced concrete slab sections from a decommissioned bridge and subsequently cast UHPC repair sections to create a composite concrete test section. In the electrical migration test to assess chloride penetration, the authors noted the effect of the steel fibers to facilitate charge being passed through the specimen between the test electrodes and modified their material to be cast without the fibers. The non-proprietary UHPC performed well in terms of charge passed (250 C) relative to a conventional concrete (2,500 C) and a proprietary UHPC performed the best (60 C) at 28-day curing. Results of the accelerated corrosion tests showed steel corrosion at the base and UHPC repair concrete interface for the proprietary UHPC concrete. The corrosion current from the anodic galvanostatic polarization appeared to concentrate in the base concrete near the composite concrete joint. The effect was less in the conventional concrete and the non-proprietary UHPC due to the relatively higher permeability that would allow greater steel polarizability.

Du et al., (2021)[13] reviewed material aspects of the durability of UHPC. The use of porous materials in the concrete mix such as that used to promote internal curing was reported to have an

impact on the total concrete porosity that can degrade the corrosion durability. The presence of concrete cracking can allow for preferential penetration of deleterious chemicals to initiate steel corrosion, but the high cement content in UHPC and the large amount of unhydrated cement can allow for some level of self-healing by sealing the crack upon subsequent hydration.

It was evident that UHPC can provide excellent bulk characteristics that may provide some benefit to mitigate carbonation-induced corrosion. As new construction, the low permeability concrete would minimize transport of moisture and aggressive chemicals. Relatively high electrical resistivity would ideally mitigate macrocell coupling. In terms of repair, it was posited that in addition to the superior mechanical behavior, the UHPC can be used to reduce the level of moisture and transport of oxygen and carbon dioxide to the substrate material to provide some level of corrosion mitigation. Some aspects of carbonation-induced corrosion are presented next.

1.2.2 Carbonation-Induced Corrosion

Corrosion Initiation

Corrosion initiation is controlled by diffusion of carbon dioxide gas into the concrete. The following are some parameters that affect the time to corrosion initiation.

The larger the concrete cover depth, the longer the transport distance that carbon dioxide has to penetrate and react with the concrete pore water and longer time to corrosion. This value can vary by design for various structural elements and for flexural steel and shear steel. This value can be identified by design drawings; however, there would always be some level of construction variability. Field testing by magnetic or GPR devices can be used to measure insitu cover depths. Cracks in the concrete even with high quality concretes can allow for localized carbonation. Deep cracks may allow for faster carbonation of concrete at rebar depths (Figure 1). [14-17]

Figure 1: Localized carbonation through concrete cracks.

The higher the cement factor, the less permeable the concrete and longer time for CO_2 transport and steel corrosion. The concrete quality for residential buildings will largely vary based on strength requirements for each structural element. Concrete quality can be measured in many different ways. In terms of carbonation including accelerated carbonation tests, air permeability and electrical resistivity have been considered.

Concrete as a hydraulic material contains pore water even if the surface seems dry. Carbon dioxide gas transport is limited in aqueous environments and must first dissolve in the liquid (via Henry's Law) to diffuse through the concrete cover. Greater internal moisture availability would allow less CO_2 transport and thus increase the time to corrosion. Exposure to higher relative humidity and surface exposure to water will better wet the concrete and increase the internal moisture content. Sheltering of concrete surfaces can create diverse exposure conditions including the effects of wetting, drying, condensation, and cyclic exposures. Measurement of the concrete internal relative humidity can be made to gage the moisture levels inside the concrete.

Carbon dioxide in the air is typically 0.04% but can be larger in areas with poor ventilation, pollution, or in industrial agricultural facilities. Greater carbon dioxide exposure would allow faster transport through the concrete and accelerate the time to corrosion.

Corrosion Propagation

Even though corrosion initiation may occur, the rate of carbonation-induced corrosion can greatly vary. The drop in concrete pore water pH associated with concrete carbonation can change the anodic behavior of the steel. For example an increase in the anodic current exchange density or a

decrease in the anodic Tafel slope will cause larger corrosion rates to develop. Furthermore, the corrosion rate can be affected by the cathodic behavior of the steel in the concrete. For example, variability in oxygen availability in wet and dry concrete can affect the corrosion rate. There is a contradicting effect of moisture presence in the concrete on the development of corrosion. For example, greater internal moisture content would inherently delay the transport of CO_2 though the cover (longer initiation times); however, once initiated, the corrosion rate will be greater (shorter propagation time). Identification of the dominant phase is necessary. Therefore the effect of material and environmental exposure conditions on the propagation time should be evaluated.

The effect of compressive loading on concrete had been considered in the technical literature. The loading on the reinforced concrete system can have different effects on corrosion. For example, compressive forces may help to close structural cracks that allow elevated penetration of water and aggressive chemical species thus increasing the initiation phase of the service life. Another example is that loads transferred to the reinforcing steel can affect defects in the rebar mill scale and the exposure of steel to the electrolyte and thus affect the anodic and cathodic characteristics of the steel.

1.2.3 Concrete Material Considerations

UHPC Carbonation Durability

Piérard et al.,(2013) [18] described the results of accelerated carbonation tests for UHPC. UHPC prisms were stored in 1% CO_2 atmosphere for up to one year. Phenolphthaleine spray on freshly fractured concrete surfaces only showed up to 2 mm depth of carbonation and a coefficient of carbonation was given as 0.1 mm/day$^{1/2}$. Andrade et al., (1996) [19] described testing of UHPC subjected to up to 100% carbon dioxide showing no carbonation after two year. After 3-year exposure, the depth was 1.5–1.7 mm. The carbonation depth was 2.5 to 4.5 times lower than those of high performance concrete and conventional concrete. [20-21]

Matos et al, (2021) [22] assessed the durability of a non-proprietary UHPC containing spent equilibrium catalyst by-product originated by the oil refinery industry, as an internal curing agent.

Transport properties and carbonation measurements were assessed. The resistance to carbonation was mainly determined by the low concrete porosity and by the reactivity of the cement phases with CO2. However, the use of the high levels of supplemental cementitious materials might deplete the portlandite content leading to an increase in carbonation. Nevertheless, the carbonation depth on the material was extremely low as determined by phenolphthalein spray on cut UHPC slices after 12 months. The carbonation depth was 0 mm after 1 year exposure.

Wang et al, (2015) [23] reviewed the UHCPC properties and indicated that the 28d carbonation depth of UHPC was very low. Long et al., (2005) [24] and Junquan Li et al., (2020) [25] indicated that carbonation could not happen on UHPC regardless of sealing, and curing conditions. Liu et al., (2003) [26] indicated that the 28-d mean depth of the carbonation of UHPC was less than 0.30 mm.

Carbonation during curing

Xian et al., (2022)[27] addressed material characteristics of concrete after carbonation used in the curing process in their research to identify the corrosion resistance of carbonation-cured concrete. Carbonation of the wet concrete during the curing stage can provide some benefits in terms of densification of the material and increasing compressive strength; however, the carbonation process results in a drop in the pore water pH. The carbonation process after the concrete is cured involves the transport of atmospheric carbon dioxide through the concrete material matrix, in part through the air void spaces and dissolution in the pore water. The reaction of the carbon dioxide and the hydroxyl ions in the concrete pore water leads to the production of carbonates and acidification of the pore water pH. Compressive strength, electrical resistivity measurements, macrocell current, and anodic galvanostatic accelerated corrosion tests were conducted on concretes subjected to carbonation curing. The carbonation-curing was shown to increase the early development of compressive strength due to the formation of calcium carbonate at the outer concrete surface. The densification of the concrete after carbonation curing was commensurately observed by the larger resolved surface electrical resistivity. This densification of the concrete also allowed for less amenable transport for chlorides whereby anodic macrocell current due to chloride-induced corrosion was delayed for the carbonation-cured concrete.

Dixit et al., (2021) [28] assessed UHPC with ground granulated blast slag and carbonation curing. The results of concrete tests indicated that carbonation curing of UHPC with slag content less than 30% resulted in reduced 28-day compressive strengths but greater compressive strengths with high slag content as cement replacement. They related the strength loss to the consumption of the already reduced calcium hydroxide content in the gel pores of concrete with the presence of the slag. The strength increased to a greater extent of carbonation at early times in fresh concrete with higher slag contents and the subsequent formation of calcium carbonate in the hydration matrix.

1.3 Research Approach

The objective of the research was to provide recommendations for practical assessment and inspection of structures that can be subject to carbonation-induced corrosion, possible remediation, as well as in-situ testing. The work was divided into three major efforts including 1) large scale concrete column testing to provide data on steel corrosion rates that can develop in concrete and to provide a framework for retrofit of carbonated concrete with corroding rebar; 2) small scale concrete testing to identify the effect of material and moisture condition environments on carbonation penetration; and 3) development of in-situ testing to identify concrete durability against carbonation. Sections 2 and 3 describes the work conducted on large scale concrete columns. Section 4 describes the work conducted on small scale concrete carbonation experiments. Section 5 describes the work to develop an in-situ testing to identify concrete durability. The final sections provide a discussion on the research finds, summary of results, and recommendations for assessing carbonation of concrete and carbonation-induced corrosion.

2. CONDUCTING TESTS ON LARGE SCALE COLUMN TEST SPECIMENS FOR ESTABLISHING TIME TO CORROSION DUE TO CONCRETE CARBONATION-WITHOUT APPLIED AXIAL LOAD

2.1 Setup

The substrate concrete for four reinforced concrete columns were cast on 1/23/23 to provide a test bed for carbonation and carbonation-induced corrosion testing. The substrate concrete was a conventional Class II concrete with a design compressive strength of 3,400 psi. Figure 2 shows the test specimens at the time of casting and demolding the formwork, prior to the casting of the repair UHPC shell.

Figure 2. Large Scale Concrete Column Test Specimens

Prior to initial casting of the substrate concrete, each concrete column had two corrosion sensors (as shown in Figure 3) installed. The corrosion sensors contain a main and auxiliary working electrode (3/8-inch diameter and 2-inch length), activated titanium rod as an embedded reference electrode, and stainless-steel rod as a counter electrode (Figure 3). The main working electrode with had a cover depth of 0.5 inch and the auxiliary working electrode had a cover of 1.75 inch.
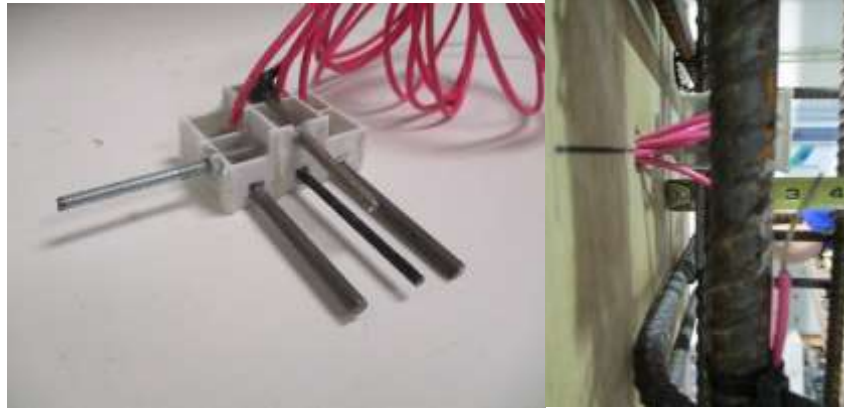
Figure 3. Corrosion sensor. Left: General view. Right: Installation in concrete column specimen formwork.

Results of the initial corrosion testing of the probes in non-carbonated concrete 1 week after casting by linear polarization resistance (LPR) method and electrochemical impedance spectroscopy (EIS) are shown in Table 1. The apparent polarization resistance, Rp' measured by LPR was corrected for the concrete solution resistance measured by EIS where Rp = Rp'-Rs. The corrosion current density (i_{corr}) was calculated as B/(Rp x A) where the Stern-Geary coefficient was assumed to be 26mV and A is the steel probe surface area. As expected, corrosion of the steel sensors in the non-carbonated concrete was low due to the development of steel passivity in the alkaline concrete pore water.

Table 1. Results of electrochemical corrosion testing of sensors (1 week after casting) 1/30/23

Column	Sensor Location	Probe	Rs (ohm)	Rp (kohm)	i_{corr} (uA/cm^2)
1	Top	W	83	664	0.0053
		A			
	Bottom	W	91	538	0.0065
		A	87	454	0.0078
2	Top	W	94	749	0.0047
		A	101	398	0.0088
	Bottom	W	83	412	0.0085
		A	73	397	0.0089
3	Top	W	63	352	0.010
		A	89	754	0.0047
	Bottom	W	91	132	0.027
		A	81	429	0.0082
4	Top	W	47	189	0.019
		A	74	1,656	0.0021
	Bottom	W	83	698	0.0050
		A	82	366	0.0096

The concrete substrate was subsequently subjected to localized early accelerated carbonation via a 4-inch diameter CO_2 injection chamber connected to a high purity CO_2 supply tank at 40 psi. The injection chamber, as shown in Figure 4 was designed, built, and tested for the research application. The time of the accelerated carbonation was determined by the time to corrosion initiation identified by monitoring of the open-circuit potential and the polarization resistance of the main corrosion electrode.

Figure 4. Carbonation Chamber

2.2 Results

Figure 5 shows the results of half-cell potential mapping of embedded longitudinal reinforcing steel in the columns after the accelerated carbonation. The potentials were measured by electrical contact of the rebar extending from the top of the concrete column to a high input impedance voltmeter and placing a copper/copper-sulfate reference electrode (CSE) at various elevations directly over each of the rebar. As expected, the rebar located directly under the injection chamber (~10-22 inches below the top of the column) showed electronegative potentials <-200 mV$_{CSE}$ indicative of active corrosion and rebar elsewhere showed electropositive potentials >-200mV$_{CSE}$ indicative of passive conditions. Correspondingly, the surface of the concrete (after roughening by sandblasting and spray with pH indicator) showed clear delineation of the drop in pH due to the accelerated carbonation directly below the injection chamber (Figure 6)
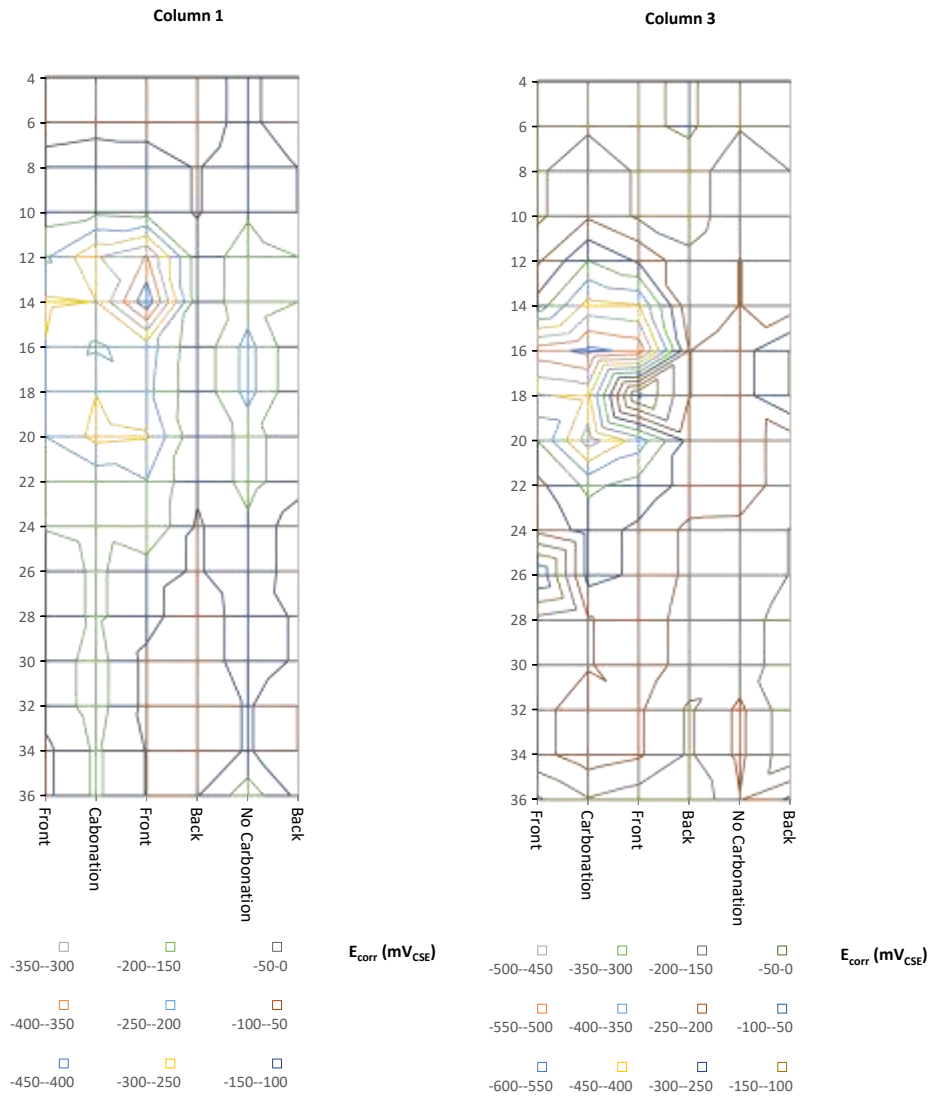
12

Column 1

Column 3

Figure 5. Half-cell Potential Mapping.

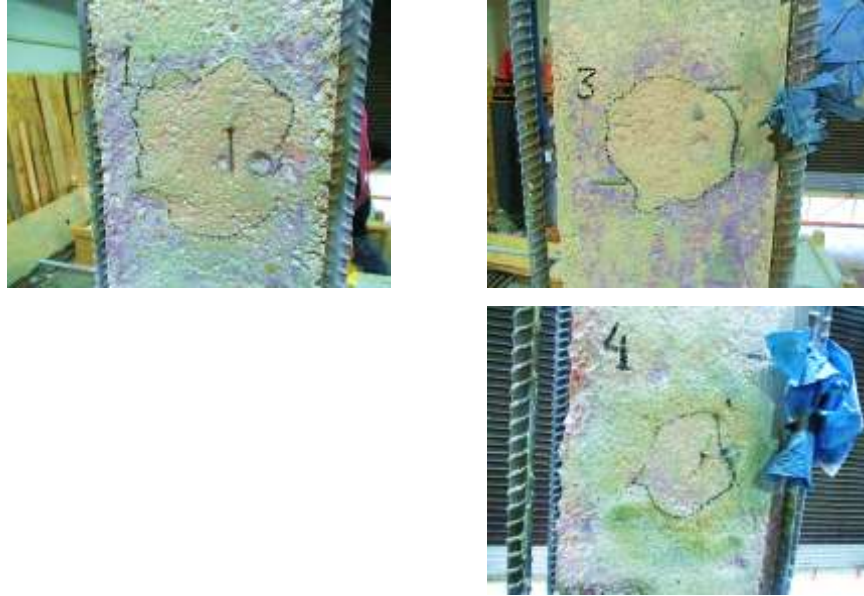y-axis: distance from top of column in inches

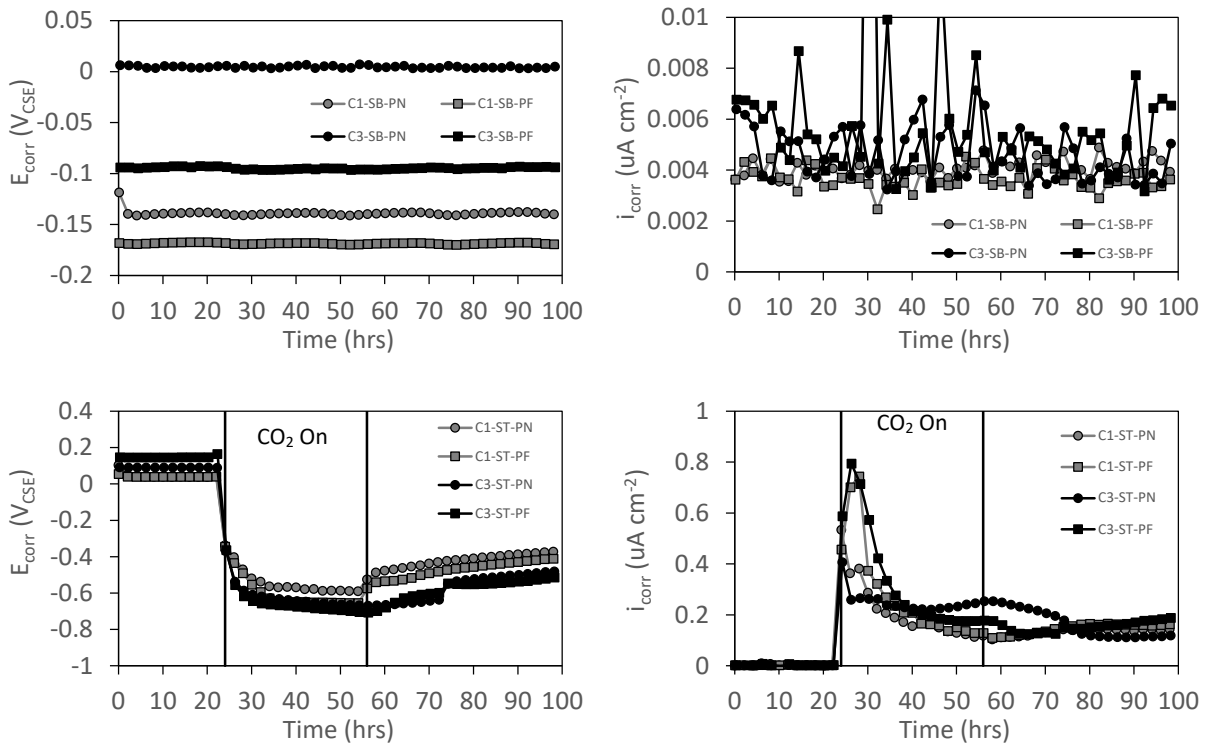Figure 6. Concrete pH after Accelerated Carbonation.

Figure 7. Corrosion Potential and Current Density during Accelerate Carbonation Testing.

Top: No Carbonation. Bottom: Accelerate Carbonation.

The corrosion potential and corrosion current density of the corrosion probes located under the injection chamber and at controlled non-carbonated sites were monitored. The corrosion potentials of the probes were initially measured with the embedded activated titanium reference electrode, but the values were corrected by calibration of the titanium reference electrode to a copper/copper-sulfate reference electrode (CSE). As shown in Figure 7, the probes located in the non-carbonation control testing showed electropositive potentials $>$-200 mV_{CSE} and low current densities <0.01 uA/cm^2, indicative of its no corrosion, passive condition. The corrosion probes under the injection chamber prior to turning on the carbon dioxide source tanks likewise showed passive conditions. The steel probes activated quickly after the carbon dioxide was introduced through the injection chamber as indicated by the sharp drop in corrosion potentials to active values and the sharp increase in corrosion current density. It was apparent that the accelerated carbonation allowed for displacement of oxygen within the pore water of the concrete as indicated by the slight increase corrosion potential and corrosion rate after the carbon dioxide source was closed and the chamber was open to atmosphere. Nevertheless, corrosion activation was sustained at approximately 0.2 uA/cm^2 (more than 20 times greater than the steel in the non-carbonated concrete). Corrosion rates were as high as 0.8 uA/cm^2 at the onset of corrosion activation.

Corrosion of the steel within the base concrete substrate would be sustained after initiation (moderated by the available oxygen in the concrete) until remediation and retrofit is made. In large scale retrofit, carbonated concrete would be identified and ideally removed as part of the repair. However, there was interest to identify any benefit afforded by encapsulation of the element with UHPC. Complete arrest of corrosion may not occur, but the beneficial characteristics of the UHPC (in addition to its structural/mechanical implications) such as low permeability, low moisture content, and high electrical resistivity may provide some mitigation in terms of the propagation stage. The outcomes of the experimental work would provide insight and empirical evidence on the benefits of retrofits made with UHPC to mitigate corrosion and further develop practical field testing for concrete durability.

3. CONDUCTING TESTS ON LARGE-SCALE COLUMN TEST SPECIMENS FOR ESTABLISHING TIME TO CORROSION DUE TO CONCRETE CARBONATION- WITH APPLIED AXIAL LOAD

3.1 Setup

One of the columns described in Section 2 was used in accelerated carbonation testing under applied compressive loadings (Figure 8). During the testing a sustained 42 kip axial load was applied to the column. The carbon dioxide was maintained in the injection chamber at 20 psi and the corrosion potential and corrosion current density were monitored (Figure 9).

Figure 8. Picture of Column Setup for Accelerated Carbonation under Axial Loading

3.2 Results

Similar to previous testing described in Section 2, the corrosion probes in the non-carbonated concrete had corrosion potentials >-200mV$_{CSE}$ and corrosion rates <0.01 uA/cm^2. After carbonation, the steel activated with corrosion potentials <-200mV$_{CSE}$ and corrosion rates

$0.2 < i_{corr} < 0.8$ uA/cm^2. In the absence of externally applied axial loads, the steel probes activated under carbonation-induced corrosion after 2 hours and 4.5 hours for the steel with 0.5 and 1.5 inch cover depths, respectively. Under the 42 kip external axial load, the initiation time was extended to 4 and 7 hours for the probes at the comparative cover depths. The delay in corrosion initiation time under axial loading appeared to be ~1.6-2 times. The presence of the external compressive forces in the concrete may provide some benefit to delay carbon dioxide ingress if microcracks in the concrete can be closed. The effect of the loading on the grains of the concrete hydration products and pore spaces require further deliberation, but the results obtained in the testing indicate some beneficial role of concrete axial loads on delaying carbon dioxide transport.
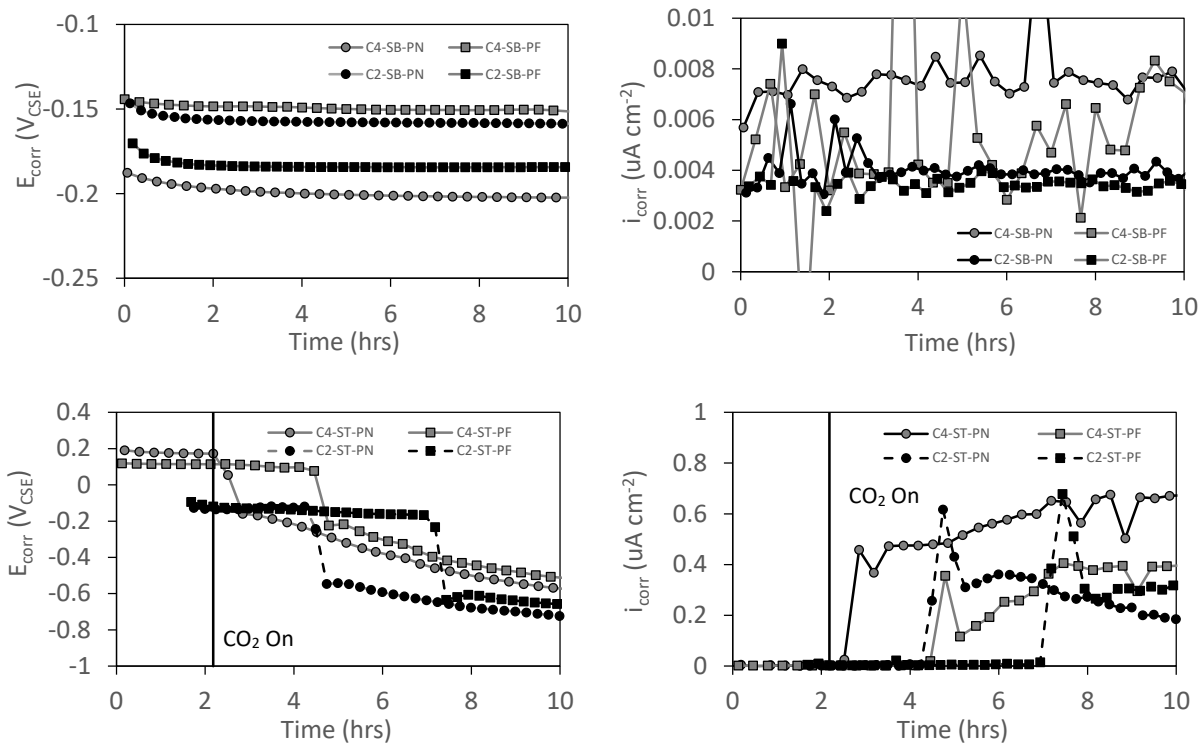

Figure 9. Corrosion Potential and Current Density during Accelerate Carbonation Testing under Axial Load. Top: No Carbonation. Bottom: Accelerate Carbonation.

4. SMALL-SCALE TEST TO ESTABLISH CONCRETE CARBONATION TIME

4.1 Setup

Concrete cylinders (4-inch and 2-inch) specimens were cast from four conventional concrete mix designs (1:1.5:3 cement, sand, coarse aggregate mix) that included a 0.5 and 0.6 water-to-cement ratio and use of #57 and #89 limestone coarse aggregate. The concretes were tested for air content of the fresh concrete. After 56 days of curing within its plastic cylinder mold, the concrete specimens were conditioned in a <35%, 75%, and >95% humidity chambers or soaked in a saturated $Ca(OH)_2$ solution. The <35% RH was controlled by use of a silica gel dessicant. The 75% RH and >95% RH was controlled with the use of saturated salts solutions in an aerated sealed chamber. The concrete were conditioned monitored until near terminal moisture conditions. The mass change, bulk electrical resistivity, electrochemical impedance spectroscopy (to measure concrete resistance and capacitance), and longitudinal resonant frequency were monitored. Figure 10 and 11 show the results of mass change and bulk electrical resistance during the concrete conditioning. As expected, greater electrical resistance developed for specimens maintained at dryer conditions.
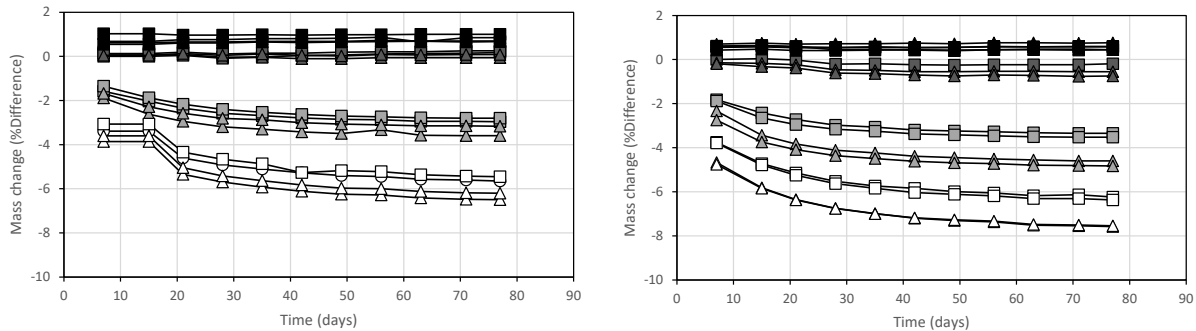

Figure 10. Mass Change during Concrete Moisture Conditioning. Left: 0.5 w/c. Right:0.6 w/c. White: 20%RH, Light Grey:75% RH, Dark Grey: 97% RH, Black: Soaked
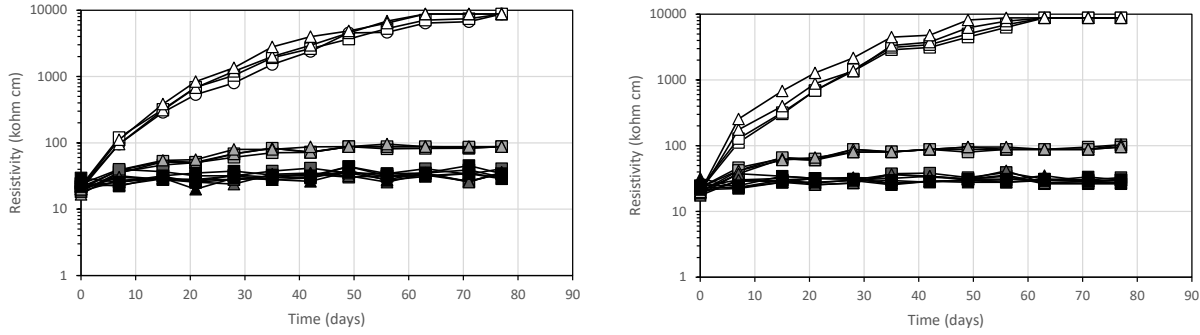
Figure 11. Bulk Resistivity during Concrete Moisture Conditioning. Left: 0.5 w/c. Right:0.6 w/c. White: 20%RH, Light Grey:75% RH, Dark Grey: 97% RH, Black: Soaked

Figure 12 and 13 show the results of electrical testing by 2-pt resistance measurements and electrochemical impedance spectroscopy. The resistivity was calculated as $\rho = R \times A/L$, where R was the measured resistance, A was the cross-sectional area of the cylinder, and L was the length of the cylinder. As expected, the electrical resistivity significantly drops in presence of high humidity and when the concrete is saturated compared to the dry conditions. Similarly, the concrete capacitance increases with the moist exposure environments due to the saturation of the concrete pores where the high dielectric characteristic of the water is detected. The longitudinal resonant frequency showed greater values for the concrete made with the larger limestone coarse aggregate and with the lower 0.5 w/c ratio mix.

Figure 14 shows good correlation between the concrete capacitance to bulk resistivity which accounts for the extent of internal moisture presence in the concrete specimens. Also, the resolved concrete Young's modulus from the longitudinal resonant frequency showed good correlation to the concrete capacitance. The results show that the internal environments in the concrete pore structure and the bulk solid is affected by the moisture content developed by the various exposure conditions.
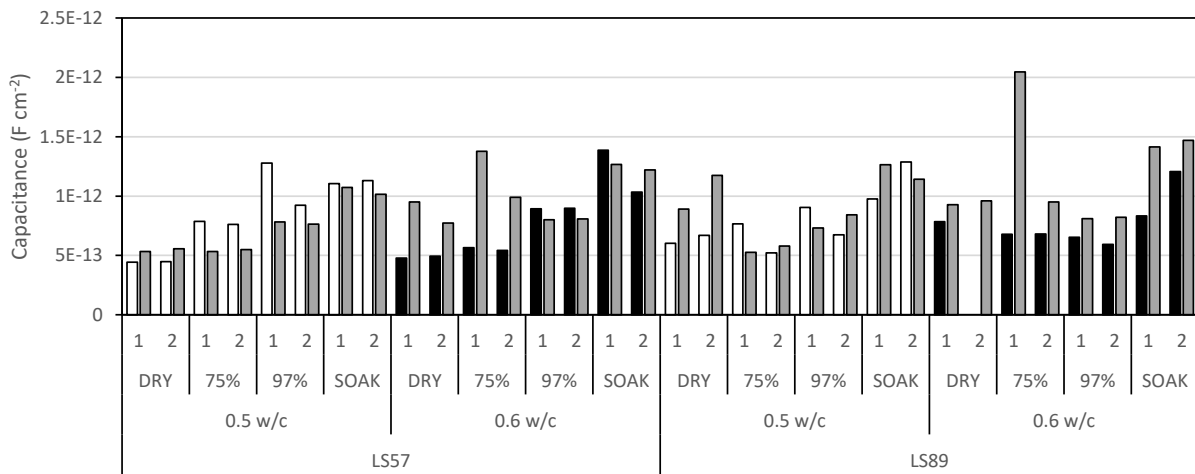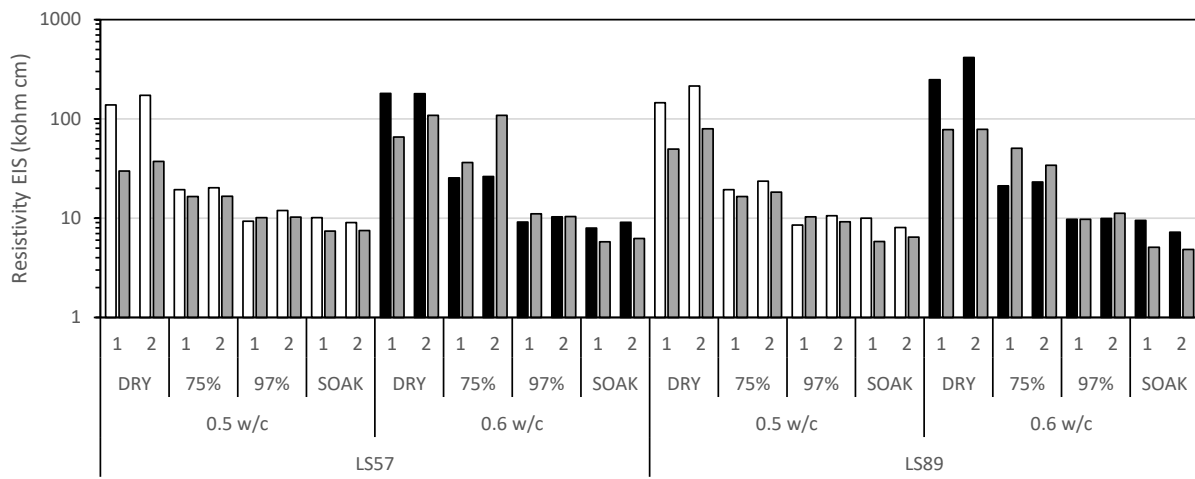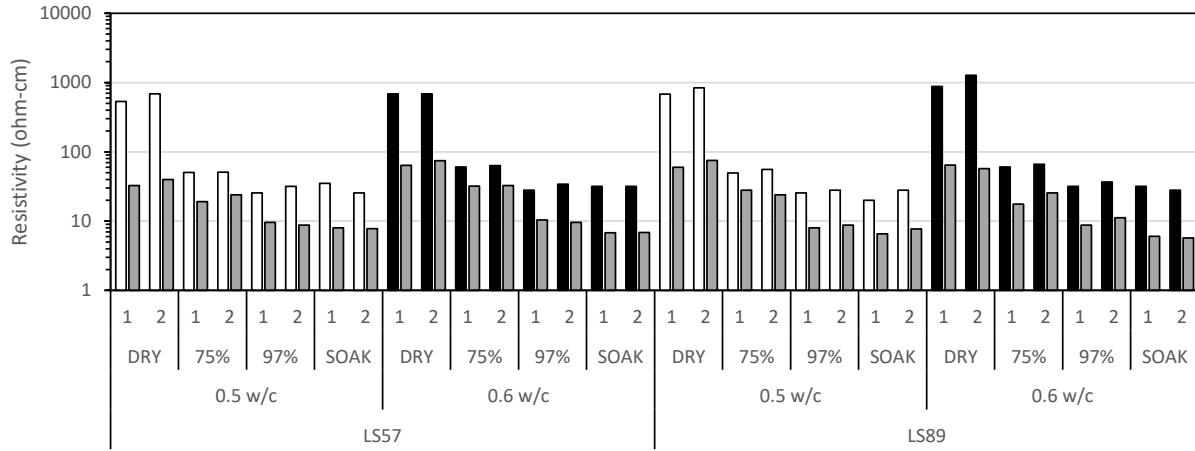
Figure 12. Comparison of Electrical Characteristics after ~23 Days of Conditioning

Figure 13. Longitudinal Resonant Frequency and Estimated Young's Modulus after ~23 days of Conditioning

Capacitance (F cm^{-2})

$y = 2E-12x^{-0.275}$
$y = 2E-12x^{-0.302}$
$y = 2E-12x^{-0.311}$
$y = 2E-12x^{-0.297}$

Resistivity (kohm cm)

E (GPa)

$y = 88.114x^{0.0325}$
$y = 86.964x^{0.0337}$
$y = 60.688x^{0.0217}$
$y = 88.562x^{0.0377}$

Capacitance (F cm^{-2})

E (GPa)

$y = 37.643x^{-0.019}$
$y = 36.063x^{-0.017}$
$y = 34.159x^{-0.009}$
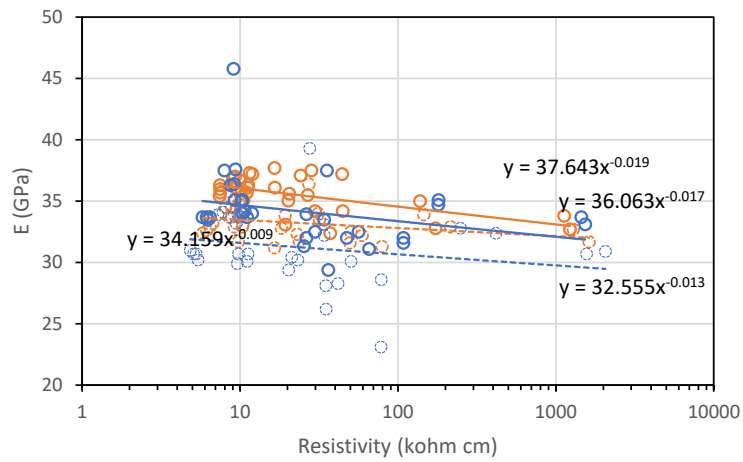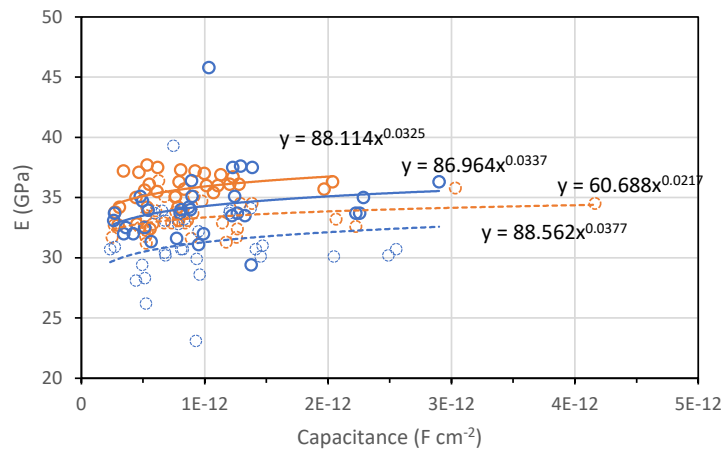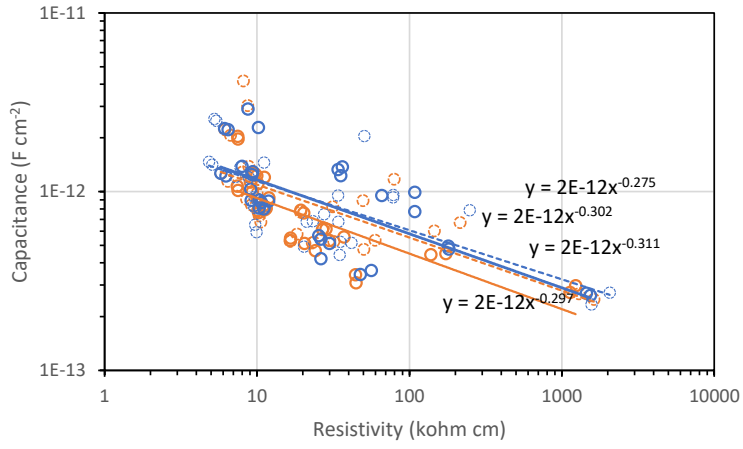$y = 32.555x^{-0.013}$

Resistivity (kohm cm)

Figure 14. Comparison of Electrical and Acoustic Characteristics.

Orange:0.5 w/c; Blue:0.6 w/c; Solid Line:#57 limestone. Dotted Line: #89 Limestone

4.2 Results

After initial material testing, the concrete cylinders were subjected to accelerated carbonation at 20 psi while maintained in their respective moisture environments. The concrete specimens that were soaked in lime water were placed in carbonation chambers conditioned at 100%RH. Figure 15 shows pictures of slices of the concrete specimens cut during various time intervals of the accelerated carbonation testing and sprayed with a pH indicator. Dark pink/purple indicate alkaline pore water conditions indicative of non-carbonated concrete. No color change in the photographs indicates regions of concrete carbonation. In each picture, the top left specimen is the 0.5 w/c with #57 limestone, the top right specimen is the 0.5 w/c with #89 limestone, bottom left specimen is the 0.6 w/c with #57 limestone, and bottom right is the 0.6 w/c with #89 limestone.

All specimens conditioned in the dry condition fully carbonated within 67 hours. None of the specimens conditioned in >95%RH or soaked/100%RH showed any indication of carbonation. For the dry and 75%RH conditions, concrete with #89 limestone aggregate had greater degree of carbonation penetration than concrete with #57 limestone aggregate.

Figure 16 shows the correlation of the electrical resistivity and capacitance and longitudinal resonant frequency to the effective radial carbonation depth measured during the accelerate carbonation testing. The effective radial carbonation depth, r' was calculated as $r'=r_o-r_{nc}'$ where r_o is the concrete specimen radius and r_{nc}' was the nominal radius of the non-carbonated concrete. The r_{nc}' value was calculated as the radius of the measured area of non-carbonated concrete paste obtained from visual analysis from digital photographs of the concrete cross-section after accelerated carbonation testing and spraying with a pH indicator. Only the dry and 75%RH test specimens are shown because no carbonation was observed for the >95%RH and Soak/100%RH specimens.

It was posited that the carbonation process would allow the precipitation of carbonates that would fill pore spaces that strengthen the concrete. This was thought to allow for greater concrete resistivity and larger resonant frequency. Some discrepant trends were observed, particularly for the dry specimens. This was thought to be due to some moisture availability from the carbon

dioxide gas even though the accelerated carbonation chamber contained dessicating media. Completion of testing to allow for carbonation of all the test specimens and subsequent moisture conditioning is required for further evaluation.

Dry: D1- 1 hr   D2- 2.5 hr   D3- 5 hr   D5- 25 hr   D6- 67 hr

75%RH: L1- 1 hr   L2- 2.5 hr   L3- 5 hr   L5- 25 hr   L7- 1 wk

95%RH: H1- 1hr   H2- 2.5 hr   H4- 10 hr
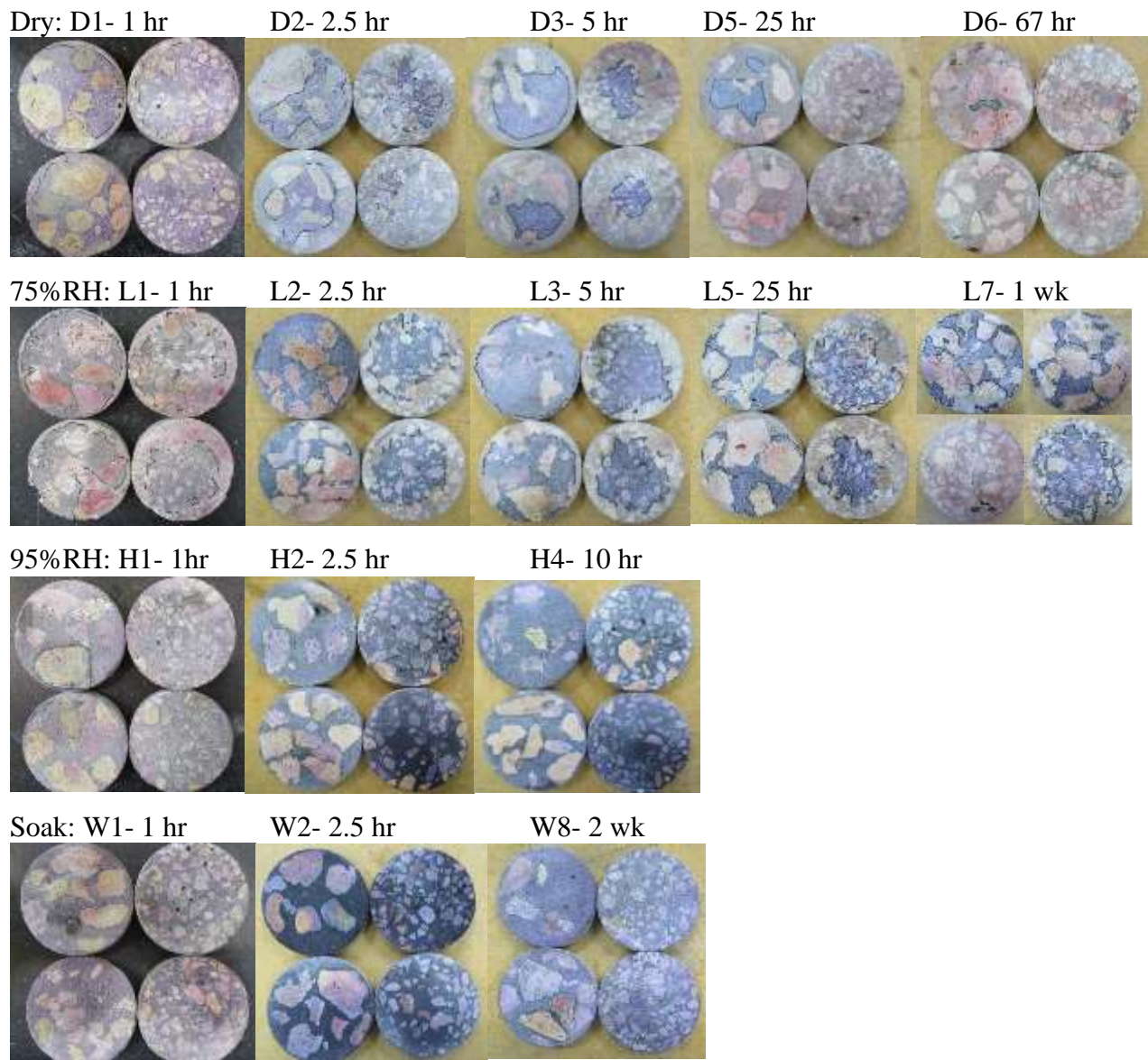
Soak: W1- 1 hr   W2- 2.5 hr   W8- 2 wk

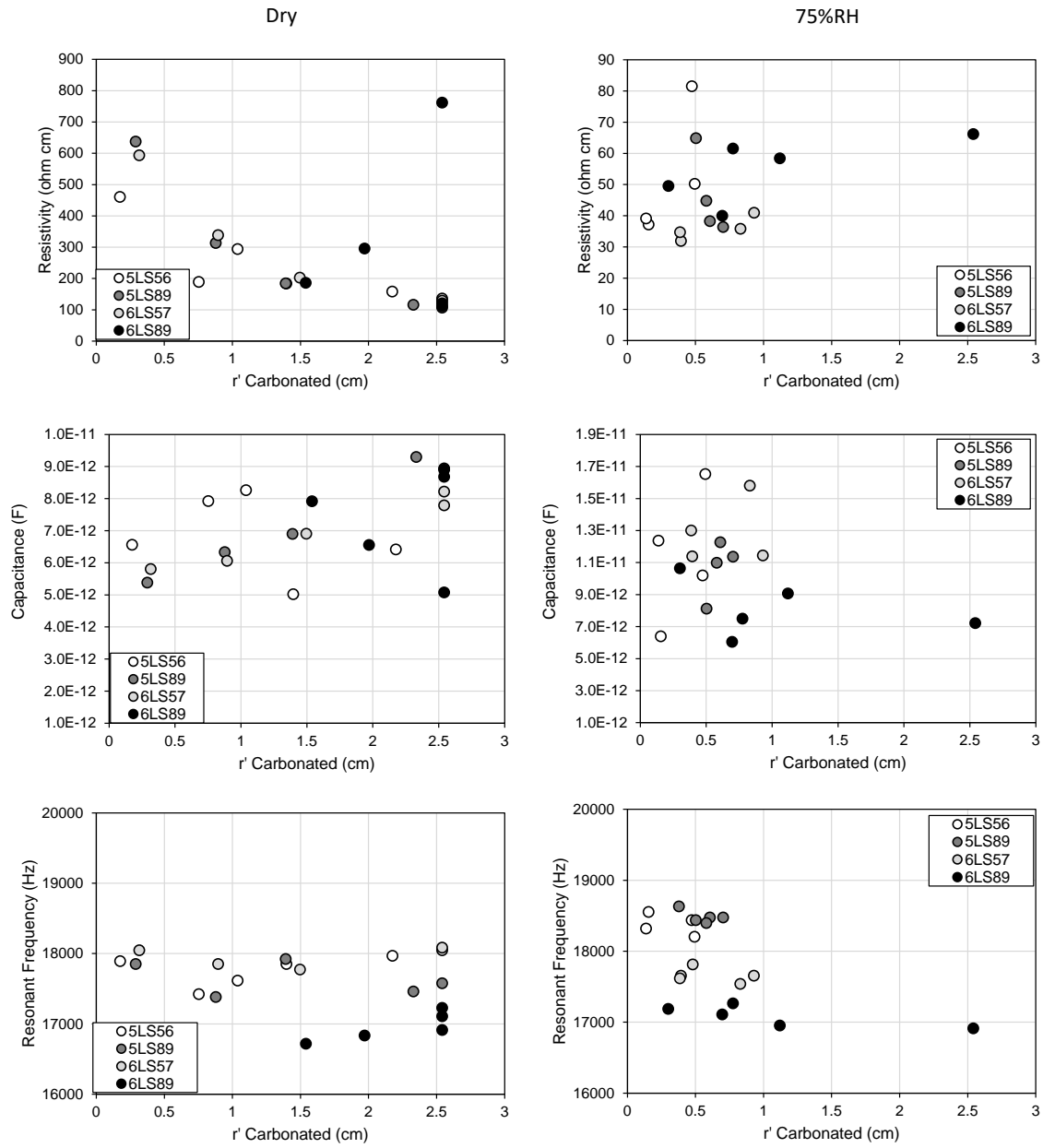Figure 15. Pictures of Concrete Specimens Cut Slices after Accelerated Carbonation

Figure 16. Correlation of Electrical Parameters and Longitudinal Resonant Frequency to Effect Carbonation Radial Depth

5. INSITU NON-DESTRUCTIVE CONCRETE TESTING

5.1 Setup

A quick non-destructive test equipment (Figure 17) being developed at FIU to assess concrete durability by measuring the change in water pressure induced at the head space of the device as moisture penetrates the concrete, relating to the concrete permeability. The same approach was used to assess changes in the concrete material due to carbonation of the concrete pore water such as the development of carbonates that may form in the pore spaces in the carbonation process. The device may potentially also detect the presence of concrete cracking that can form after corrosion initiation.

Figure 17. Water Pressure Drop Concrete Test Apparatus

Concrete cylinders (4 inch diameter) were cast with concrete made from a 1:1.5:3 cement, sand, coarse aggregate mix with 0.5 and 0.6 water-to-cement ratio. Coarse aggregates were either #57 or #89 size. Cylinders were conditioned in <35%, 75, >95%RH, or soaked in lime water. After 56 days of concrete hydration within the plastic cylinder mold, and additional time of moisture conditioning, the cylinders were tested by subjecting one transverse face of the concrete to 200 psi of water and measuring the pressure drop for up to 20 minutes. An example of the test results in shown in Figure 18.
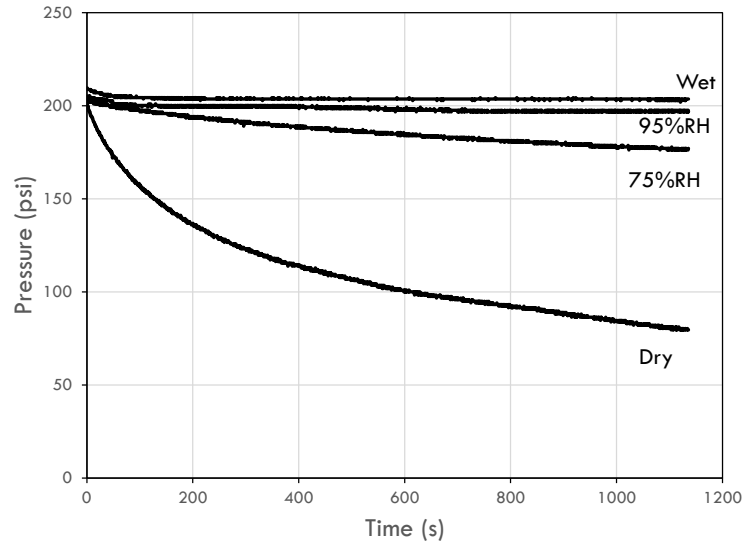
Figure 18. Example of Water Pressure Drop Test Results

5.2 Results

The water pressure drop consistently showed an exponential decay in the pressure with time. This behavior was attributed to water penetration through the concrete pore spaces with time as shown in Figure 19. Following mass and energy balance,

$$S = -Q \qquad\qquad\qquad \text{Eq. 1}$$

$$p_B = \tfrac{1}{2}\, \rho\, V_A{}^2 \qquad\qquad\qquad \text{Eq. 2}$$

where S is the water storage within the water pressure vessel, Q is the discharge through the concrete, p_B is the water pressure in the vessel, ρ is the density of water, and V_A is the water velocity through an idealized pore; $p_B(t) = [\sqrt{p_o} - Kt/2]^2$ where p_o is the initial water pressure and K is a decay factor. However, this idealized expression did not provide good description of the actual measured pressure drop. An additional term, k relating to water transport through partly saturated pores with time was introduced. The differential equation expressing the change in pressure was introduced as

$dp/dt = -K \exp(-kt) \times \sqrt{p}$
                                                            Eq. 3

and

$p_B(t) = [\sqrt{p_o} - K + K \exp(-kt)]^2.$
                                                            Eq. 4

The function expresses the water pressure with time due to an initial pressure p_o, pore saturation factor k, and a pressure decay factor K. Factors k and K ideally would be characteristic to the concrete material and exposure conditions. Figure 20 shows an example of fitting test data to Eq. 4, and Figure 21 shows the good correlation between the apparent pressure drop measured after 20 minutes from the initial ~200 psi to K.
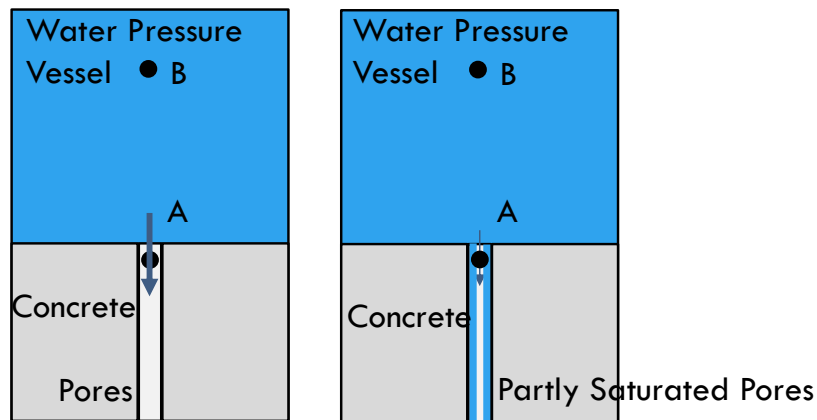

Figure 19. Schematic of Idealized Water Transport through Concrete.
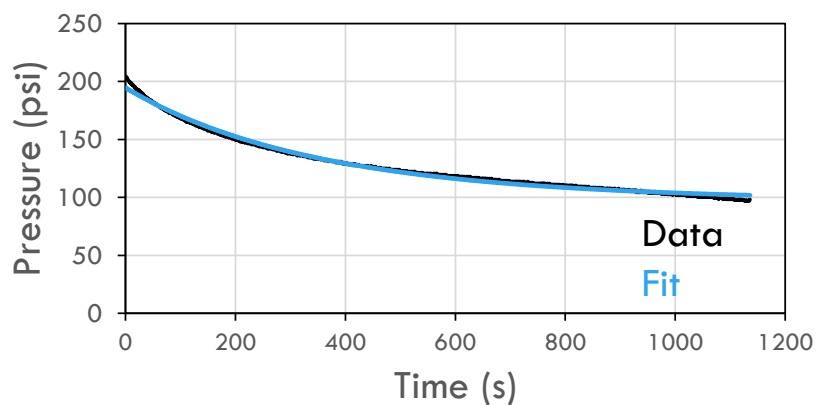
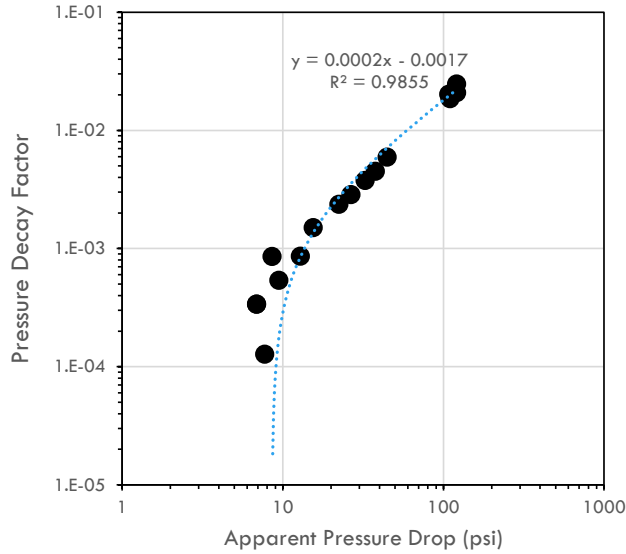

Figure 20. Example of Data Fitting.

Figure 21. Correlation of Measured Apparent Pressure Drop to Pressure Decay Factor.
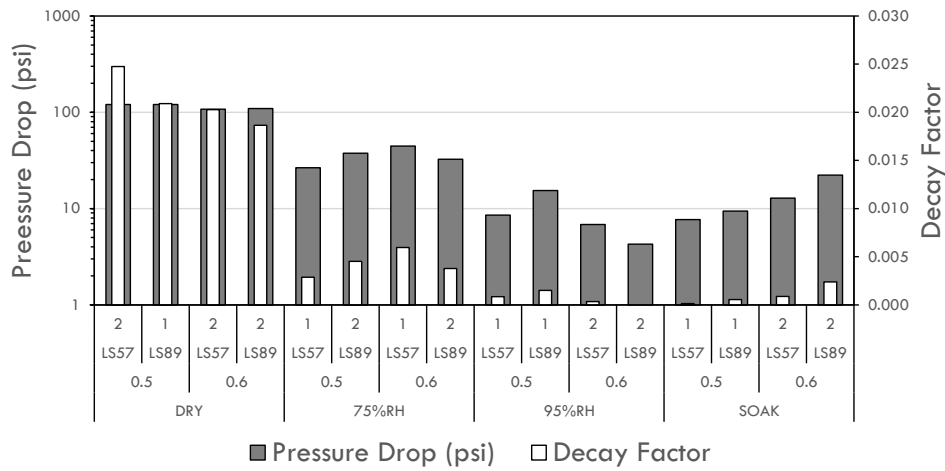

Figure 22. Results of Water Pressure Drop Test

Figure 22 shows the outcome of the water pressure drop test. The internal concrete moisture content had strong influence on the water transport and greater pressure drop was apparent for the concrete conditioned in <35%RH. Figure 23 shows the correlation of the pressure decay factor to the resolved concrete electrical properties.
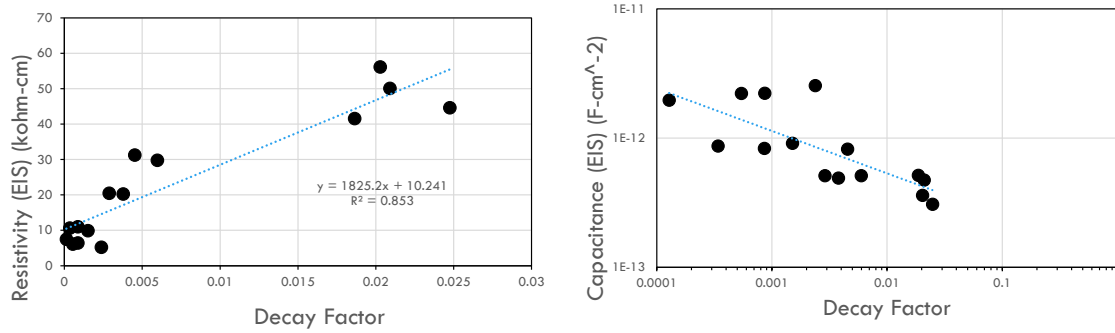
Figure 23. Correlation of Pressure Decay Factor to Concrete Electrical Properties

Concrete electrical properties have been promoted to characterize concrete permeability and overall durability. The bulk resistivity has been demonstrated by some researchers to characterize both the concrete solid microstructure as well as the pore water within. Likewise, the capacitance would be influenced by the microstructure as well as the amount of water within the pore spaces. For example, an increase in capacitance can be related to the presence of water that has a larger dielectric constant ε, than for the solids following the relationshiop $C = \varepsilon \, \varepsilon_o A/d$ where A and d are idealized area and lengths of pores and ε_o is the permittivity of free space.

6. RESEARCH OUTCOMES

6.1 Large Scale Concrete Columns

In the dry indoor laboratory conditions, the corrosion rate of steel in the non-carbonated concrete was measured to be on average ~0.01 uA/cm^2. In the carbonated concrete, the corrosion rate ranged from 0.2-0.8 uA/cm^2. From Faradaic conversion, these rates correspond to steel loss of up to 0.001 mm\yr (0.25 mils/yr) corrosion.

In presence of the 42 kip external compressive force, the corrosion rates were similar; however, the time to corrosion initiation was delayed in time by a factor of 1.6-2.

A test bed for concrete retrofit of carbonated concrete with actively corroding reinforcing steel and instrumentation for corrosion monitoring was developed. Shell repair including the use of UHPC can be implemented for additional study. Figure 24 shows the columns being prepared for the shell repair by initial surface roughening by sandblast to provide up to ¼ inch roughness and the placement of the welded steel stirrups. Final corrosion testing after the shell concrete has been cast and after loading can be made to identify the efficacy of retrofit techniques and materials to mitigate carbonation-induced corrosion.

Figure 24. Column Sandblasting and Shell Retrofit

6.2 Small Scale Concrete Specimens

The concrete cast with the different water-to-cement ratio, limestone aggregate size, and conditioned in various moisture environments had different electrical and acoustic characteristics that are inter-related with the concrete microstructure and internal moisture content. These parameters have impact to the extent of concrete carbonation and the extent of corrosion activity.

The concrete specimens conditioned in the 95%RH and soak/100%RH conditions maintained in extended accelerated carbonation conditioning for up to 1 month of continuous carbonation of near 100% CO_2 at 20 psi did not yield any significant carbonation penetration due to the slow rate of CO_2 penetration through the pore water. It was evident that additional time was required for concrete carbonation. With prolonged exposure, carbonation penetration rates may be obtained and be used to assess corrosion initiation times for various concrete mixes subjected to the various moisture environments.

Concrete carbonation for the concrete specimens maintained in the dry condition fully carbonated within 67 hours in 100% CO_2 environments at 20 psi. Significant concrete carbonation occurred for the concrete specimens maintained at 75%RH. Figure 25 shows the effective radial depth of carbonation for the concrete specimens held in the dry and 75%RH conditions. Specimens with higher w/c and with smaller coarse aggregate showed faster carbonation penetration.
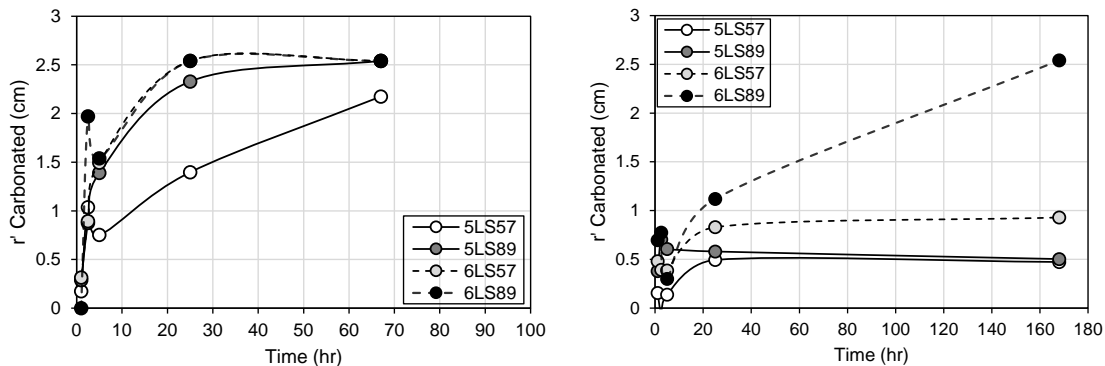

Figure 25. Effective Radial Depth of Carbonation during Accelerated Carbonation Testing

6.3 Non-Destructive Testing

Development of a novel insitu water pressure drop test method is ongoing. The test methods has been demonstrated to be sensitive to the internal moisture content of the concrete. Models based on mass and energy conservation have been developed to predict the water pressure drop for concrete with different materials and environmental exposure and ideally can be used to identify concrete characteristics related to permeability and thus susceptibility to carbonation.

7. RECOMMENDATIONS

From the outcomes within the scope of the limited research described in the report, the following recommendations for assessment of concrete carbonation and carbonation-induced corrosion are made.

- Inspection timing for concrete carbonation should consider concrete materials including the water-to-ratio, aggregate type and size, and internal moisture presence. Concrete with greater continuous paths through the cement paste allow for faster carbonation penetration. This includes dryer concretes (such as those tested in <35% and 75%RH. Concretes with smaller coarse aggregates were also shown to provide faster carbonation rates.

- The carbonation-induced corrosion rate can greatly vary depending on material, internal moisture content, and internal oxygen availability. Even though corrosion initiation times may be slower in concretes with greater internal moisture content, its corrosion propagation can be significantly greater. Additional testing to assess corrosion propagation times for carbonated concrete under various levels of internal moisture is warranted.

- The influence of chlorides in the concrete should also be considered for corrosion risk assessments of coastal structures. The drop in concrete pore water pH due to carbonation and presence of chlorides can create aggressive corrosion conditions.

- Accelerated carbonation testing of large scale concrete columns showed that the corrosion rates of steel in carbonated concrete can be moderated by the availability of oxygen within the concrete pore water at the steel rebar surface. This effect can be considered in structural retrofits including shell repair using low permeability materials such as UHPC.

- Insitu non-destructive testing can be employed for concrete inspections for concrete durability. Among those, testing to assess concrete permeability, carbonation, and corrosion rates should be considered.

8. REFERENCES

1. M. Stefanoni, U. Angst, B. Elsener. "Corrosion rate of carbon steel in carbonated concrete–A critical review." Cement and Concrete Research 103 (2018) pp.35-48.

2. EN, B. S. (2000). 206-1 Concrete-Part 1: Specification, performance, production and conformity. British Standards Institution.

3. H.G. Russel, B.A. Graybeal, "Ultra-High Performance Concrete: A State-of-the-Art Report for the Bridge Community." Federal Highway Administration; McLean, VA, (2013).

4. ASTM C1202-19, "Standard Test Method for Electrical Indication of Concrete's Ability to Resist Chloride Ion Penetration" West Conshohocken, PA: ASTM.

5. E. Shahrokhinasab, D. Garber, "Development of "ABC-UTC Non-Proprietary UHPC Mix." Final Report# ABC-UTC-2016-C2-FIU01-(2021).

6. ASTM C1760-12, "Standard Test Method for Bulk Electrical Conductivity of Hardened Concrete", West Conshohocken, PA: ASTM.

7. ASTM C157/C157M-17, "Standard Test Method for Length Change of Hardened Hydraulic-Cement Mortar and Concrete", West Conshohocken, PA: ASTM.

8. A.Valikhani, K. Lau, "Field Demonstration, Instrumentation, and Monitoring of Accelerated Repair Using UHPC Shell" Final report, ABC-UTC-2016-C1-FIU 02, (2021).

9. PRW, Floyd, "Development Of Non-Proprietary Uhpc Mix" Final report, OU-2016-2-1-(2020).

10. G.U. Chunping, S. Wei, G.U.O Liping, and W. Quannan. "Effect of Curing Conditions on the Durability of Ultra-High Performance Concrete under Flexural Load," Journal of Wuhan University of Technology, April 2016, 278-285 (2016)

11. T. Looney, M. Leggs, J. Volz, R. Floyd, "Durability and corrosion resistance of ultra-high performance concretes for repair." Construction and Building Materials, 345 (2022) 128238.

12. ASTM C666-97, "Standard Test Method for Resistance of Concrete to Rapid Freezing and Thawing" ,West Conshohocken, PA: ASTM.

13. J. Du, W. Meng, KH. Khayat, Y. Bao, P. Guo, Z. Lyu, H. Wang, " New development of ultra-high-performance concrete (UHPC)." Composites Part B: Engineering, 224 (2021) 109220.

14. A. A. Sagüés, K. Lau, R. G. Powers, R. J. Kessler. "Corrosion of Epoxy-Coated Rebar in Marine Bridges—Part 1: A 30-Year Perspective." Corrosion 66 (2010) pp. 065001–065001–13. doi: https://doi.org/10.5006/1.3452397

15. K. Lau, A. A. Sagüés, R. G. Powers. "Corrosion of Epoxy-Coated Rebar in Marine Bridges—Part 2: Corrosion in Cracked Concrete." Corrosion 66 (2010) pp. 065002–065002–16. doi: https://doi.org/10.5006/1.3452398

16. K. Lau, A.A. Sagúés, "Corrosion Evaluation of Bridges with Epoxy-Coated Rebar." Final Report to Florida Department of Transportation, Contract No. BD544-23, (2009). https://rosap.ntl.bts.gov/view/dot/17037

17. K. Lau, A.A. Sagues, "Corrosion of steel in locally deficient concrete." Final Report to Florida Department of Transportation, Contract No. BD544-31, (2009) https://rosap.ntl.bts.gov/view/dot/17429

18. J. Piérard, B. Dooms, N. Cauberg, " Durability evaluation of different types of UHPC." In Proceedings of the RILEM-fib-AFGC International Symposium on Ultra-High Performance Fiber-Reinforced Concrete, Marseille, France, (2013) pp. 1-3.

19. M.C. Andrade, M. Frías, B. Aarup, "Durability of UltraHigh Strength Concrete: Compact Reinforced Composite (CRC),"Proceedings of the Fourth International Symposium on the Utilization of High-Strength/High-Performance Concrete 2 (1996), Paris, France, Ed., de Larrard, F. and Lacroix, R, pp. 529–534

20. C. Alonso, M. Castellote, I. Llorente, C. Andrade, "Ground water leaching resistance of high and ultra high performance concretes in relation to the testing convection regime," Cem. Concr. Res. 36 (2006) pp. 1583–1594.

21. M. Schmidt, E. Fehling, "Ultra-high-performance concrete: research, development and application in Europe," ACI Special publication 228 (2005) pp. 51–78.

22. A.M. Matos, S. Nunes, C. Costa, JLB. Aguiar, " Durability of an UHPC containing spent equilibrium catalyst." Construction and Building Materials, 305 (2021) 124681.

23. D. Wang, C. Shi, Z. Wu, J. Xiao, Z. Huang, Z. Fang, " A review on ultra high performance concrete: Part II. Hydration, microstructure and properties." Construction and Building Materials, 96 (2015) 368-377.

24. G.C. Long, Y.J. Xie, P.M. Wang, Z.W. Jiang, "Properties and micro/mecrostructure of reactive powder concrete," J. Chin. Ceram. Soc. 4 (2005) pp. 456–461.

25. J. Li, Z. Wu, C. Shi, Q. Yuan, Z. Zhang, " Durability of ultra-high performance concrete–A review." Construction and Building Materials, 255 (2021) 119296.

26. S.F. Liu, W. Sun, W. Lin, J.Z. Lai, "Preparation and durability of a high performance concrete with natural ultra-fine particles," J. Chin. Ceram. Soc.11 (2003) pp. 1080–1085.

27. X. Xian, D. Zhang, H. Lin, Y. Shao, " Ambient pressure carbonation curing of reinforced concrete for CO_2 utilization and corrosion resistance." Journal of CO_2 Utilization, 56 (2022) 101861.

28. A. Dixit, H. Du, S. Dai Pang, "Carbon capture in ultra-high performance concrete using pressurized CO_2 curing." Construction and Building Materials, 288 (2021) 123076.